Data Driven Ergonomic Design of a Passive Spinal Exoskeleton

Aaron Griffith*
* University of Illinois at Chicago, Chicago, USA, Email: agrif5@uic.edu

***Abstract*—This study introduces a data-driven methodology for the ergonomic design of a passive spinal exoskeleton tailored to human spinal curvature and movement. Motion capture data from multiple participants were processed using Mokka and MATLAB to yield averaged spinal trajectories. These curves were analyzed using an optimization algorithm (MATLAB's fmincon) to determine ideal exoskeleton link configurations under geometric and anatomical constraints. A secondary evaluation using the Analytic Hierarchy Process (AHP) weighted ergonomic fit, cost, and durability to rank candidate designs. The results identified a nine-link configuration as the most effective balance between range of motion and comfort, achieving minimal root mean square error (RMSE) relative to the averaged spinal curvature. Additional engineering considerations—including power delivery via a 24 V 15 Ah LiFePO4 battery system, voltage regulation through a buck converter, and control via Arduino—were integrated to support future active functionality. This approach demonstrates how biomechanics, optimization, and engineering design can converge to produce anatomically informed exoskeletons with real-world applicability.**

***Index Terms*—Data Driven, Ergonomic, Spinal Exoskeleton, MATLAB**

I. Introduction

Exoskeletons are emerging as promising assistive technologies in healthcare, industrial, and rehabilitation domains [27]. One major challenge in their development is ensuring ergonomic compatibility, as anatomically congruent design is essential for adoption. Poor ergonomic fit can discourage use regardless of a device's functional performance [28]. Drawing inspiration from fundamental principles of spine anatomy—including the segmentation into cervical (C1–C7), thoracic (T1–T12), lumbar (L1–L5), and sacral (S1) vertebrae [26]—and their respective ranges of motion, we aim to develop a spine-aligned passive exoskeleton that mirrors the natural posture and movement of the human spine.

The spine exhibits complex, multi-axis motion. Each vertebra contributes to six degrees of freedom: flexion/extension, lateral bending, axial rotation, and translations along the x-, y-, and z-axes. White and Panjabi [29] report that these motions are further stabilized by major muscle groups such as the erector spinae, which generate and resist forces across all planes. Understanding these biomechanical properties is essential for developing passive assistive structures that maintain both safety and comfort.

Ergonomics are emerging as a critical factor in the adoption and usability of exoskeletons. One of the most significant barriers to widespread use is user discomfort. Devices that do not conform to individual anatomy are typically rejected, regardless of their functional benefits. Many existing designs lack the flexibility and personalization required to ensure comfort, contributing to limited user acceptance. By prioritizing ergonomic considerations, adoption rates can be substantially improved. Many current designs fall short in this regard, lacking the flexibility and personalization needed to ensure comfort. By prioritizing ergonomic considerations, we can dramatically increase the likelihood that individuals will choose to incorporate exoskeletons into their daily routines. When combined with the functional benefits of exoskeletons—such as reduced musculoskeletal strain, gait support, and enhanced strength—an ergonomic design becomes essential to user acceptance. [30]

Historically, many exoskeleton designs have relied on intuitive and iterative, trial-and-error development processes. While these methods have yielded functional systems, they often lack the precision and repeatability of a data-informed approach. Our work aims to bridge this gap by integrating human motion capture data into the design process. By mapping spinal motion through biomechanical trials and applying optimization algorithms to determine ideal exoskeleton link placements, we can move beyond intuition toward a rigorously engineered solution. This data-centric strategy not only enhances ergonomic performance but also establishes a robust foundation for future innovations in spinal exoskeleton development.

The remainder of this paper is organized as follows: Section II reviews relevant literature; Section III defines the design problem; Section IV describes the methodology; Section V presents analysis and results; and Section VI concludes the study with proposed directions for future work.

II. Research

To define a meaningful engineering problem, a thorough review of existing literature was conducted. Foundational insights into spinal anatomy and kinematics were drawn fromTroke et al. [1], Hajibozorgi and Arjmand [2], Feipel et al. [3], and Frobin et al. [4], who together establish benchmarks for lumbar, thoracic, and cervical motion. Figure 1 illustrates a segmented view of the human spine.

Design precedents include Zhang et al.'s spring-based passive exoskeleton [5], a full-body support system from Rol and Sankai [6], and a beam-based spinal support by Kong et al. [7]. While mechanically functional, these systems do not account for personalized ergonomic alignment, a critical focus of this project.

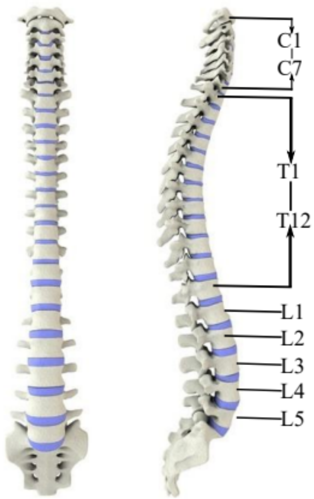

Fig. 1: Anterior and lateral views of the vertebral column, showing cervical, thoracic, lumbar, and sacral regions. Adapted from Frobin et al.

The six degrees of freedom stemming from the spine and its movement is critical in creating an ergonomic spinal exoskeleton design. [26] Troke et al. and colleagues reported the following ranges:

Rotational Motion:

Flexion/Extension: Cervical (60–80°), Thoracic (25–45°), Lumbar (20–35°)
Lateral Bending: Cervical (30–45°), Thoracic (20–30°), Lumbar (20–25°)
Axial Rotation: Cervical (30–45°), Thoracic (20–30°), Lumbar (20–25°)

Translation Movements:

Anterior–Posterior: 1–3 mm
Lateral Translation: 1–3 mm
Vertical Translation: 1–2 mm

These flexibility parameters are crucial insight for our design parameters. To build onto that foundation our design must satisfy the following:

Spinal Frame

Follows the natural curve and flexibility of the human spine
Lightweight and rigid material

Thoracic and Lumbar Support

Needs to stabilize the upper body to reduce strain, while all exoskeleton segments are connected

Neck Connection

Secure
Flexible
Allow for flexion, extension, and rotation.

Multiple design options were evaluated during the conceptual phase of the exoskeleton. One key consideration was the use of articulated joints—mechanical connections that permit relative motion between rigid components, closely mimicking the movement capabilities of anatomical joints. These joints enable controlled motion, transmit forces effectively, and provide the necessary degrees of freedom required for spinal articulation. Common types include hinge joints, ball-and-socket joints, and Cardan (or universal) joints, which are frequently used in biomechanical applications to simulate joint behavior. Figure 2 illustrates an example of such a joint. In addition to articulated mechanisms, spring-assisted joints were investigated [24]. These joints incorporate elastic components to support or resist motion, reducing the physical effort required by the user and offering potential energy storage and return, thereby enhancing comfort and mechanical efficiency.

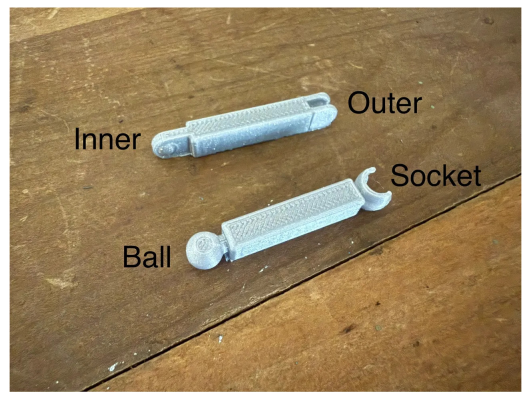

Fig. 2: Illustration of an articulated joint featuring both ball-and-socket and concentric inner–outer configurations. These configurations demonstrate the degrees of freedom and motion versatility commonly required in biomechanical exoskeleton designs.

Spring-assisted joints were also investigated as a means of enhancing passive support. These mechanical joints incorporate elastic elements, such as springs, to support or resist motion, thereby reducing the required force or energy input from the user or actuator. By assisting user movement and decreasing muscular effort, these joints can store and release energy during motion cycles, ultimately improving user comfort. While spring-assisted joints may slightly limit the overall range of motion compared to fully articulated mechanisms, they offer a significant advantage in energy efficiency and fatigue reduction. A representative example of a spring-assisted joint is shown in Figure 3 [24].

Lastly, a hybrid backpack-style exoskeleton design was investigated. This wearable assistive configuration integrates structural components—such as joints, passive supports, and wiring—along the spine within a harness or vest-like system. Worn similarly to a conventional backpack, the system is intended to distribute load evenly while maintaining ergonomic

Fig. 3: Depiction of a spring-assisted joint incorporating an elastic element to support and resist motion. This configuration enables partial energy recovery and reduces user effort by supplementing joint movement with stored elastic potential.

alignment. The design accommodates modular cylindrical components for vertical spinal support and provides structural pathways for safely routing electrical wiring.

Several engineering constraints were considered to ensure feasibility. Material strength was critical to support both the exoskeleton and the biomechanical loads imposed by the human body. Weight minimization was also prioritized to maintain comfort and reduce user fatigue. Mechanically, the device required robust but adjustable interfaces to connect securely to the torso while preserving mobility. Thermally, materials needed to be both breathable and fire-resistant in the event of electrical failure.

To guide material selection, existing designs from commercial backpack manufacturers such as Camelbak and Lululemon were reviewed. Nylon was considered for the outer shell and shoulder strap surfaces due to its strength-to-weight ratio. Mesh fabrics were proposed for areas requiring ventilation, such as shoulder straps. For electrical insulation and fire resistance, materials like Nomex, Kevlar, and wool were evaluated for surrounding high-voltage components [20], [25]. Figure 4 presents a comparative overview of structural textile properties suitable for the exoskeleton's wearable frame.

Strong Fabrics	Light Fabrics	Durable Fabrics	Fire-Resistant Fabrics
Nylon	Nylon	Nylon	Fire Resistant Polyester
Cordura	Polyester	Canvas	Kevlar
Neoprene	Spandex	Polyester	Fire Resistant Cotton
Canvas	--	Kevlar	--
Kevlar	--	--	--

Fig. 4: Comparison of structural and thermal properties of candidate fabrics for exoskeleton integration. Materials such as nylon, mesh, Nomex, and Kevlar were evaluated based on strength, breathability, and fire resistance to inform backpack-style harness design.

Incorporating a reliable battery system is a critical design requirement for enabling future active functionality in the passive spinal exoskeleton. Key electrical considerations include voltage, current, energy capacity, size, configuration, and safety. Active exoskeletons often rely on sufficient electrical power to drive motors and actuators, and a 24 V power supply was selected to balance performance, efficiency, and compatibility. Most wearable robotics components operate within a 12–48 V range; a 24 V configuration provides adequate torque and speed while reducing current draw, thereby minimizing resistive losses and allowing the use of thinner wires and smaller components. This voltage also supports extended operational life before recharging becomes necessary.

Beyond voltage, the selected battery capacity was 15 amp-hours (Ah), based on estimated power demands, desired runtime, and expected system losses. Typical actuators used in dynamic tasks like walking or lifting draw between 2–5 A, making 15 Ah sufficient for medium-to-long usage durations. This capacity also accommodates transient high-torque loads, preventing voltage sag and potential motor brownouts.

Battery configuration was another important consideration. Batteries connected in series increase total voltage, while parallel configurations raise total capacity. Multiple battery chemistries were evaluated to meet both performance and structural constraints. Alkaline options, such as A27 and D-cell batteries, were dismissed due to excessive unit counts and physical infeasibility. Lithium-ion chemistries emerged as the most viable solution, particularly due to their high energy density, low self-discharge, and widespread use in electric vehicles, aerospace, and robotics.

Among lithium-ion variants, two options were compared: Nickel Manganese Cobalt (NMC) and Lithium Iron Phosphate (LiFePO4 or LFP). NMC batteries are known for their high energy output and moderate cycle life, but have lower thermal stability. In contrast, LiFePO batteries offer superior safety, longer cycle life, and greater thermal and chemical stability, making them better suited for wearable applications. As a result, the Headway LiFePO4 40152S battery (17 Ah, 3.2 V per cell) was selected. These cells are 1.57 inches in diameter and 6.5 inches in length, and can be connected in series to meet the 24 V system requirement while maintaining a manageable form factor. Figure 5 shows the selected battery model.

To interface the battery system with future active components such as actuators or motors, an Arduino microcontroller was selected. Arduino is an open-source electronics platform built around easy-to-use hardware and software, commonly employed in prototyping, robotics, sensing, and control applications [15]. Each board includes a microcontroller, digital and analog I/O pins, voltage inputs, and a USB interface for programming. The platform is programmed using a C/C++-based language and is known for its accessibility and flexibility, making it ideal for rapid development and testing of embedded systems. Figure 6 shows the Arduino UNO R3, the specific model used for this application.

Given the Arduino's recommended operating voltage range of 7–12 V and an absolute maximum input of 20 V, a voltage step-down solution is necessary to safely interface it with the 24 V battery system. To accomplish this, a buck

Fig. 5: Two Headway LiFePO4 40152S batteries (17 Ah, 3.2 V) with screw terminals. These cells were selected for their safety, energy capacity, and physical compatibility with the wearable frame.

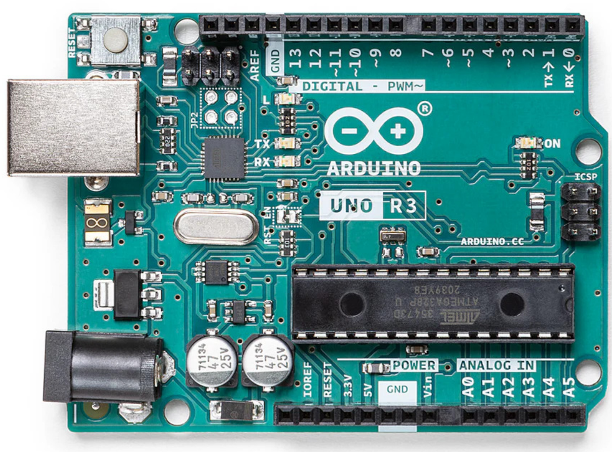

Fig. 6: Top-down view of an Arduino UNO R3 board, used for microcontroller-based control and system integration.

converter was selected. A buck converter is a high-efficiency DC-DC voltage regulator that reduces a higher input voltage to a lower, stable output voltage. It operates using high-speed switching components—such as transistors, inductors, and capacitors—to regulate energy flow through pulse-width modulation.

These converters typically achieve efficiencies of 80–95 percent, making them compact and suitable for embedded systems. In this application, the buck converter steps down the 24 V supply to 5 V, which is then routed to the Arduino's 5 V input pin. This ensures safe operation while maintaining compatibility with other low-voltage control components. Figure 7 shows the buck converter used for this voltage regulation task.

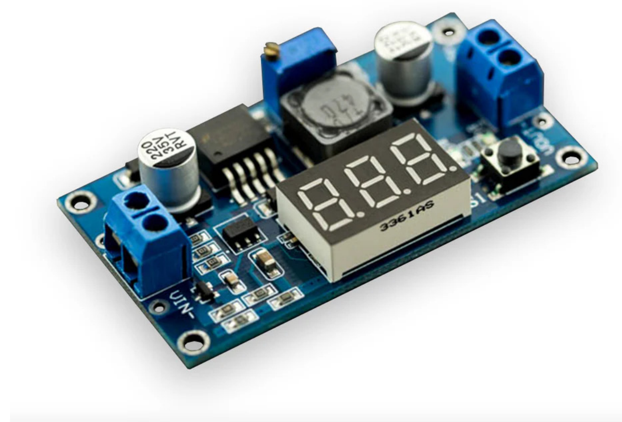

Fig. 7: Isometric view of the buck converter used to step down the 24 V battery output to a stable 5 V input for the Arduino.

With the selection of the batteries, Arduino, and buck converter complete, the next step was to determine a safe and functional wiring configuration. To interconnect the batteries and components, ring terminals and spade connectors were utilized. A ring terminal features a closed circular loop that is secured to a terminal post via a screw or bolt, while the wire is crimped into the opposite end. Spade connectors, by contrast, have a U-shaped design that allows for quick attachment under a screw terminal without removing the screw entirely.

To achieve the desired 24 V output, the batteries were connected in series. This was done by linking the positive terminal of the first battery to the negative terminal of the second, continuing this pattern until the final battery. The overall positive output from the final battery was connected to the motor's power input, and the negative terminal from the first battery was connected to the motor's ground.

Additionally, the buck converter was integrated to safely power the Arduino. The same final positive terminal was routed to the input of the buck converter, and the first negative terminal was connected to its ground. The buck converter then stepped down the voltage to a regulated 5 V, which was delivered to the Arduino's input pin. Figure 8 illustrates the complete wiring layout for this configuration.

With these design considerations established, the next phase of the study involved investigating spinal mapping techniques and motion capture data. Armitano et al. provided a valuable precedent by successfully generating spinal trajectories through experimental motion trials. After establishing contact with the authors, permission was granted to utilize their dataset, which served as the foundation for this study's design methodology and validation.

Building on an understanding of spinal biomechanics, segmental motion, and previous design efforts, this research

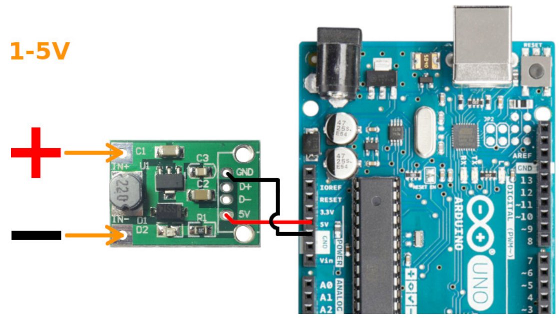

Fig. 8: Wiring configuration connecting series-wired batteries to both a buck converter and an Arduino UNO. The buck converter reduces the 24 V battery output to 5 V for safe Arduino operation.

focused on determining optimal link placements for a spinal exoskeleton composed of n discrete segments, each of length l. The objective was to identify a spatial configuration that maximizes both range of motion and ergonomic comfort. MATLAB was used to generate an average spinal curvature from the motion capture dataset, and an optimization algorithm (fmincon) was implemented to compute ideal link positions while adhering to anatomical and geometric constraints.

III. Methodology

To implement the design methodology, it was first necessary to obtain high-quality motion data for spinal mapping. The dataset used in this research was originally developed by Armitano et al. and provided in the C3D file format. C3D is a standardized public-domain format commonly used in biomechanics, gait analysis, and animation. These files contain detailed three-dimensional marker trajectories along with auxiliary analog signals from systems such as force plates and electromyography sensors.

To visualize and extract relevant data from the C3D files, the open-source software Mokka (Motion Kinematic and Kinetic Analyzer) was utilized [17]. Mokka is a cross-platform application designed for the analysis of motion capture data, offering both 2D and 3D visualization. Key features relevant to this study included the ability to track individual markers in three-dimensional space over time, plot spatial coordinates, and export the motion capture data to Microsoft Excel for subsequent processing and analysis in MATLAB.

Using Mokka, approximately 90 motion capture trials were imported and processed from a total of 11 participants. Each subject was outfitted with markers strategically placed along the spine and instructed to either stand still or walk along a straight path. For every trial, 12 spinal markers were tracked: one positioned at the sacrum, five along the lumbar region, five on the thoracic spine, and one at the cervical level. The data were then exported from Mokka into Microsoft Excel, organized by participant, trial type (standing or walking), and corresponding marker sets for further analysis in MATLAB.

With the data systematically organized, the next phase involved analysis, visualization, and optimization using MATLAB—a high-level computing environment widely used for numerical computation and algorithm development. The exported Excel data were imported into MATLAB, where they were normalized and processed to compute the average two-dimensional coordinates (X and Y) of each spinal marker. These averaged coordinates were then used to generate a representative spinal curve for each individual trial.

To generate a representative spinal model for optimization, trial plots were first consolidated by computing the mean position of each spinal marker across all trials for each participant using Microsoft Excel. These participant-specific average curves were then combined to form a single aggregate spinal curve representing the average spinal geometry across all subjects and trials. This aggregate curve served as the reference trajectory for the optimization process.

Exoskeleton link placement was optimized using MATLAB's Optimization Toolbox, specifically the fmincon function, which is well-suited for solving constrained nonlinear minimization problems. The objective was to minimize the sum of squared errors (SSE) and root mean square error (RMSE) between the spinal curve and the proposed link configuration, subject to the following constraints:

1) The number of links (n) must be between 3 and 10
2) Each link must have a length between 25 mm and 100 mm
3) The first link must start at the base of the spinal curve
4) The final link must end at the top of the spinal curve
5) All links must connect consecutively without skipping z-values along the spinal spline

By executing fmincon under these constraints, the algorithm identified the optimal number, lengths, and spatial placements of links that best conformed to the spinal curve. Once the optimal configuration was determined, geometric and angular parameters were calculated using the following equations:

$$L_i = \sqrt{(Y_{i+1} - Y_i)^2 + (Z_{i+1} - Z_i)^2}, \quad \text{for } i = 0, \dots, N-1. \tag{1}$$

Equation 1: This equation calculates the Euclidean distance (segment length) between two consecutive points in a 2D plane, where Y and Z represent the vertical and depth coordinates, respectively.

$$\theta = \cos^{-1}\left(\frac{\mathbf{v}_i \cdot \mathbf{v}_{i+1}}{\|\mathbf{v}_i\|\|\mathbf{v}_{i+1}\|}\right) \tag{2}$$

Equation 2: This equation computes the angle θ_i between two adjacent vectors $\mathbf{v}_i$ and $\mathbf{v}_{i+1}$ using the dot product formula. The numerator represents the dot product of the vectors, while the denominator normalizes by the product of their magnitudes.

While the optimal link configuration minimized geometric deviation from the spinal curve, it did not account for external factors such as material cost or structural durability. To incorporate these additional design criteria, the Analytic Hierarchy

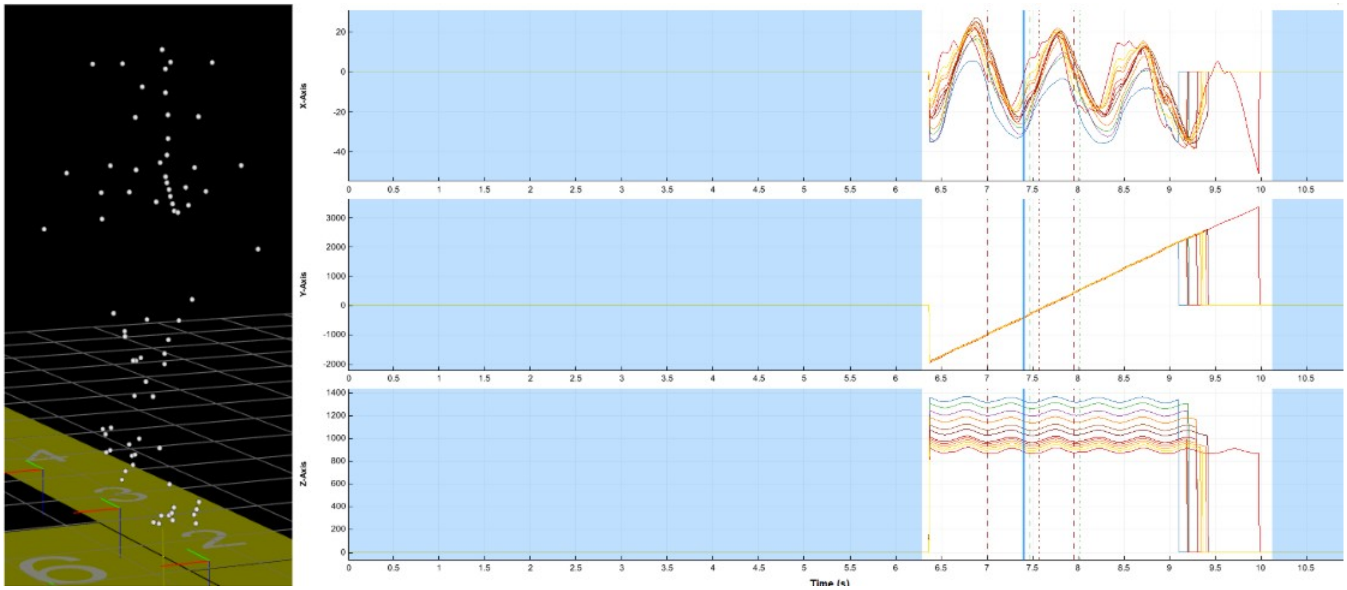

Fig. 9: Screenshots from Mokka showing 3D body map tracking (left) and 2D marker trajectory plots (right). These tools enabled precise extraction and visualization of spinal marker motion over time.

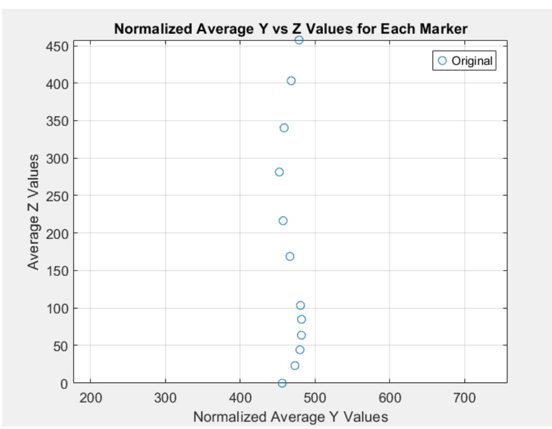

Fig. 10: Visualization of spinal marker trajectories in the X–Y plane using MATLAB. The plot represents averaged marker coordinates used to generate individual spinal curves.

Process (AHP) was employed. AHP is a structured multi-criteria decision-making method that breaks down complex problems into a hierarchical model of goals, criteria, and alternatives. It utilizes pairwise comparisons and a standardized numerical scale (typically ranging from 1 to 9) to assess the relative importance of each criterion. A weight vector is then derived by calculating the principal eigenvector of the resulting comparison matrix [23].

In this study, the following weights were assigned to the design objectives: RMSE (0.714), cost (0.143), and durability (0.143). This weighting reflects the central importance of minimizing root-mean-square error (RMSE) between the modeled and experimental spinal trajectories, which directly influences the ergonomic accuracy of the exoskeleton. RMSE was prioritized to ensure the anatomical fidelity of the design, while cost and durability—though essential for manufacturability and long-term viability—were weighted equally at a lower value. This balanced weighting scheme allowed for performance optimization without sacrificing practical feasibility.

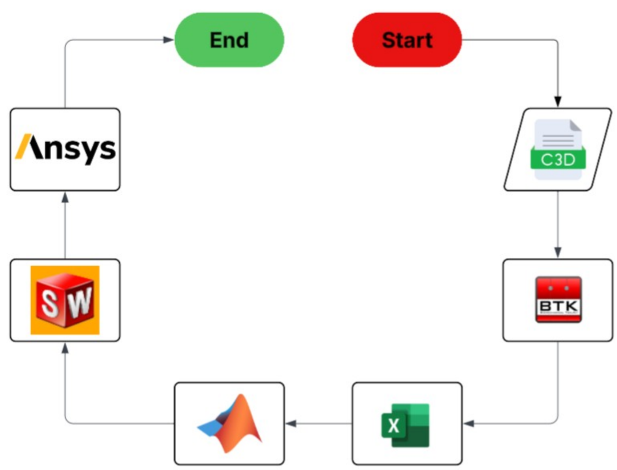

Fig. 11: Workflow diagram summarizing the data processing, optimization, and mechanical design phases of the exoskeleton development process.

Following the completion of the optimization routine, the next phase involves transitioning to mechanical design using SolidWorks. SolidWorks is a parametric, feature-based 3D computer-aided design (CAD) software developed by Dassault Systèmes, widely used for the design and simulation of mechanical components and assemblies. In this project, SolidWorks is used to model precise mechanical links, joints, and structural frames; simulate the motion and load conditions across components; visualize assembly interactions; and export detailed technical drawings and part files for manufacturing and 3D printing [21].

IV. Analysis and Design

To assess spinal curvature across different movement contexts, four types of spinal mapping plots were analyzed: (i) Participant 3's second walking trial, (ii) Participant 7's average standing trial, (iii) the aggregate average standing spine map, and (iv) the aggregate average walking spine map. This comparative analysis underscored the importance of a robust participant pool and multiple trials to produce accurate, data-driven insights into spinal kinematics.

Figure 12 illustrates the relationship between the number of exoskeleton links (n) and the resulting root mean square error (RMSE). The results show a substantial 13.2 mm reduction in RMSE when increasing the link count from n=5 to n=6. Beyond six links, the improvement becomes more gradual, with only a 1.8 mm gain observed from n = 6 to n = 10. These findings suggest that six links represent a critical threshold for achieving acceptable ergonomic fit, while configurations exceeding nine links offer diminishing returns relative to the increased mechanical complexity, alignment sensitivity, and fabrication cost.

--- Optimization Summary Table ---

NumLinks	SumSqError	RMSE
3	14610	15.605
4	20747	16.104
5	24846	15.763
6	781.23	2.5515
7	388.78	1.6664
8	198.4	1.1135
9	132.19	0.85695
10	108.53	0.73664

Fig. 12: Optimization results using MATLAB's `fmincon` function showing the sum of squared error (SSE) and root mean square error (RMSE) for link counts ranging from $n = 3$ to $n = 10$. The data illustrates a sharp RMSE reduction from $n = 5$ to $n = 6$, followed by diminishing returns beyond $n = 9$.

Figures 13a and 13b highlight the postural differences between standing and walking conditions. As expected, the standing spine is more vertically aligned, while the walking posture displays a slight anterior lean—consistent with momentum-induced adjustments in spinal orientation during locomotion.

Figures 14a and 14b further illustrate these trends by comparing individual spine maps from representative MATLAB

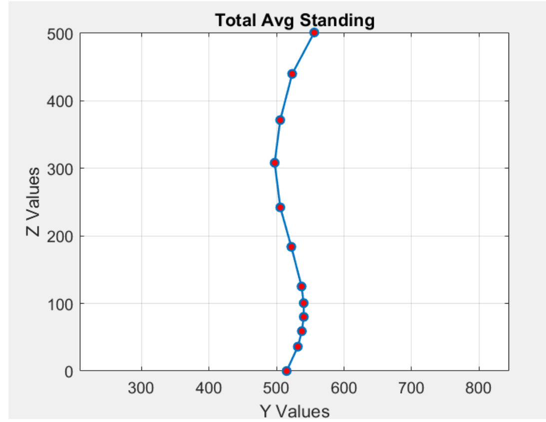

(a) Average standing spinal map derived from all participant trials.

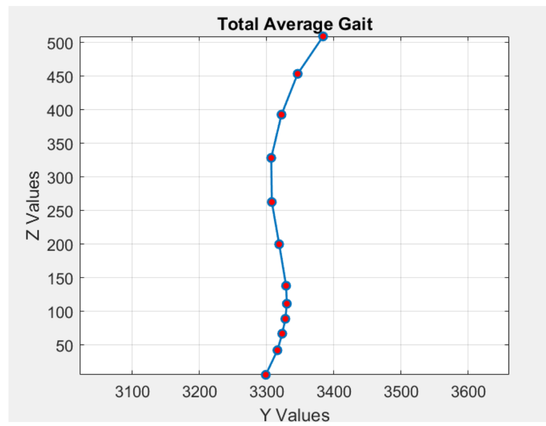

(b) Average walking spinal map derived from all participant trials.

Fig. 13: Comparison of average spinal trajectories during standing and walking. The standing posture shows a more vertical alignment, while the walking posture exhibits a forward lean consistent with locomotion.

trials. The standing trial shows reduced curvature and a more upright posture, while the walking trial reveals greater spinal flexion, particularly in the lumbar region.

With all spinal maps analyzed, we proceeded to the MATLAB-based fmincon optimization routine to evaluate the relationship between link count and geometric fidelity. As shown in Figure 12, the optimization results reveal a substantial reduction in root mean square error (RMSE) when increasing the number of links from n=5 to n=6, with a 13.21 mm improvement in average distance between the modeled exoskeleton and the spinal curve. In contrast, configurations with fewer than six links exhibit significantly larger deviations, making n=3 to n=5 unsuitable for ergonomic design due to excessive spacing between the exoskeleton and spinal trajectory.

Beyond six links, the reduction in RMSE becomes increasingly marginal. The improvement from n=6 to n=10 is only 1.82 mm, indicating diminishing returns in performance. While additional links may enhance anatomical fidelity, they also introduce increased mechanical complexity, greater align-

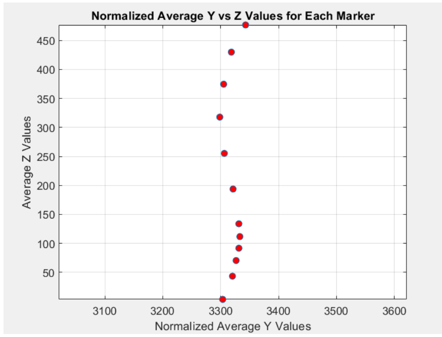

(a) Walking trial spinal map generated in MATLAB.

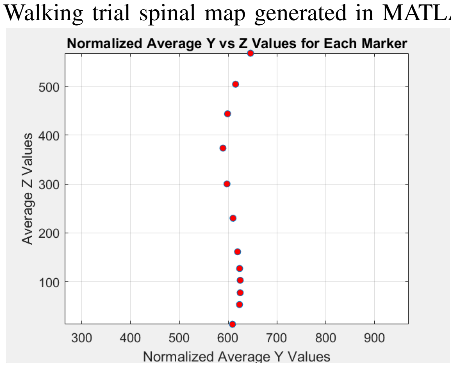

(b) Standing trial spinal map generated in MATLAB.

Fig. 14: Representative spinal maps from individual walking and standing trials. The walking posture shows a forward lean and increased curvature, especially in the lumbar region.

ment sensitivity, and higher fabrication costs. Based on these trade-offs, the ergonomic "goldilocks zone" appears to lie between six and ten links. The final selection within this range—balancing performance with manufacturability—is discussed in the subsequent section.

Figure 12 also provides insights into the geometric characteristics of the optimized link configurations, specifically in terms of segment length and inter-link angle. Link lengths range from 25 mm to 100 mm, with angles between adjacent links spanning from 2.91° to 15.80°. The longest segment—Link 3—consistently measures 100 mm across configurations and is positioned near the transition between the lumbar and thoracic regions, corresponding to the most linear portion of the spine. The recurrence of this length suggests a biomechanically flatter region in that area, supporting the use of longer segments where curvature is minimal.

Conversely, the largest angular transition (15.80°) occurs between Links 1 and 2 in the lumbar region, which exhibits the highest degree of spinal curvature. This observation supports future design strategies that employ variable segment density: shorter links in high-curvature zones (e.g., lumbar and cervical regions) and longer links in flatter regions (e.g., mid-thoracic). Additionally, as the number of links n increases, the reduction in average inter-link angle suggests improved fidelity in curvature replication. Lower angles between adjacent links may help distribute pressure more evenly and reduce localized stress concentrations—an important consideration for comfort and long-duration wear.

Across all configurations, the mean and median link lengths were 52.28 mm and 47.58 mm, respectively, while the mean and median inter-link angles were 10.2° and 10.7°.

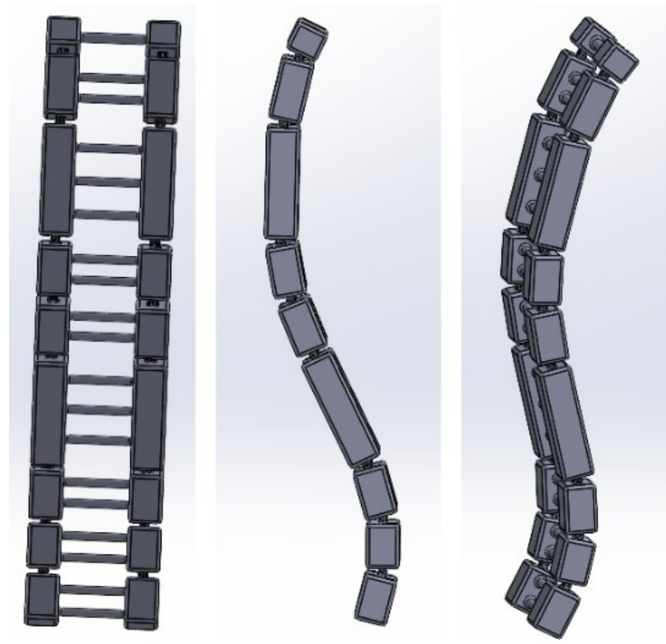

Fig. 15: SolidWorks model of the passive spinal exoskeleton shown from back, side, and isometric views. This configuration reflects the nine-link optimized design, illustrating curvature conformity and anatomical alignment.

Evaluating broader trends across configurations with n=6 to n=10, a clear pattern emerges in both link lengths and inter-link angles. As the number of links increases, the average link length decreases—dropping by approximately 14 percent from n=6 to n=7, followed by a gradual reduction of about 1 percent per additional link. Cumulatively, this results in a 34.97 mm decrease in average link length from n=6 to n=10. Among the frequently recurring segments (Links 0 through 5), Link 0 is consistently the shortest, while Link 3 is the longest—showing a length difference of 38.83 mm. Notably, Link 3 often reaches the upper limit of 100 mm, indicating a relatively linear section of the spine and suggesting that future designs might benefit from a relaxed upper bound for improved conformity.

A parallel trend is observed in inter-link angles. The average angle between adjacent links decreases by approximately 10–15 percent with each incremental increase in n, though the decline is not strictly linear. The largest average angle consistently occurs between Links 0 and 1—corresponding to the high-curvature lumbar region—while the smallest angle is found between Links 3 and 4 in the thoracic region. These patterns reinforce the need for adaptive segment density and angular resolution to replicate spinal curvature accurately.

To finalize the exoskeleton design, the Analytic Hierarchy Process (AHP) was employed to incorporate multi-criteria decision-making beyond geometric optimization. The evaluation considered three weighted factors: root mean square error

--- Weighted-Sum Final Results ---

NumLinks	SSE	RMSE	Cost	Durability	RMSENorm	CostNorm	DurabNorm	CompositeScore
6	781.23	2.5515	300	91	1	0	1	0.71429
7	388.78	1.6664	350	88	0.51232	0.25	0.75	0.43737
8	198.4	1.1135	400	85	0.20768	0.5	0.5	0.2912
9	132.19	0.85695	450	82	0.066294	0.75	0.25	0.26164
10	108.53	0.73664	500	79	0	1	0	0.28571

Fig. 16: AHP-based weighted score matrix generated in MATLAB for link configurations ranging from $n = 3$ to $n = 10$. The nine-link configuration achieved the lowest composite score, indicating optimal performance across RMSE, cost, and durability criteria.

(RMSE) with a weight of 0.714, material cost with 0.143, and structural durability with 0.143. These weights reflect the prioritization of ergonomic conformity while maintaining practical considerations for manufacturability and longevity. As illustrated in Figure 16, the nine-link configuration yielded the lowest composite score of 0.26164, designating it as the most balanced and optimal solution based on the specified criteria.

V. Conclusion

This research presents a comprehensive, data-driven framework for the design of an ergonomically optimized passive spinal exoskeleton. By integrating motion capture data, MATLAB-based numerical optimization, anatomical constraints, and multi-criteria evaluation via the Analytic Hierarchy Process (AHP), we developed a methodology that yields biomechanically sound and user-centered outcomes. The resulting nine-link configuration achieved the best trade-off between spinal conformity, material cost, and structural durability, minimizing root mean square error (RMSE) relative to the spinal curve.

This computational approach was further supported by detailed engineering design, including battery system selection, joint architecture, form factor analysis, and embedded electronics integration. Key decisions—such as employing a 24V, 15Ah LiFePO4 battery, voltage regulation via a buck converter, and Arduino-based control—were grounded in performance, efficiency, and safety considerations specific to wearable assistive devices.

Nonetheless, several limitations should be acknowledged. The motion capture dataset consisted of only eleven participants and twelve spinal markers, limiting both biomechanical resolution and population generalizability. The current model does not account for soft-tissue compliance, dynamic loading, or fatigue-related effects. Ergonomic validation was also limited in scope.

Future work will address these gaps by increasing marker density, expanding participant trials, and incorporating soft-tissue modeling, real-time actuator simulation, and dynamic compliance features. Prototyping and load-bearing validation will further advance the design toward practical deployment.

Ultimately, this study advances spinal exoskeleton design from trial-and-error engineering toward an evidence-based, user-informed paradigm—paving the way for more adaptable, comfortable, and functional human-robot interaction.

VI. Acknowledgments

The author gratefully acknowledges the mentorship of Salvador Echeveste, whose guidance and technical feedback were invaluable throughout the course of this project. Appreciation is also extended to Dr. Pranav Bhounsule, Head of the Robotics and Motion Laboratory at the University of Illinois at Chicago.

References

[1] M. Troke, A. P. Moore, F. J. Maillardet, and E. Cheek, “A normative database of lumbar spine ranges of motion,” Manual Therapy, vol. 10, no. 3, pp. 198–206, Aug. 2005, doi: https://doi.org/10.1016/j.math.2004.10.004.

[2] M. Hajibozorgi and N. Arjmand, “Sagittal range of motion of the thoracic spine using inertial tracking device and effect of measurement errors on model predictions,” Journal of Biomechanics, vol. 49, no. 6, pp. 913–918, Apr. 2016, doi: https://doi.org/10.1016/j.jbiomech.2015.09.003.

[3] V. Feipel, RondeletB., J.-P. Le Pallec, and M. Rooze, “Normal global motion of the cervical spine”:, Clinical Biomechanics, vol. 14, no. 7, pp. 462–470, Aug. 1999, doi: https://doi.org/10.1016/s0268-0033(98)90098-5.

[4] W. Frobin, G. Leivseth, M. Biggemann, and P. Brinckmann, “Sagittal plane segmental motion of the cervical spine. A new precision measurement protocol and normal motion data of healthy adults,” Clinical Biomechanics, vol. 17, no. 1, pp. 21–31, Jan. 2002, doi: https://doi.org/10.1016/s0268-0033(01)00105-x.

[5] H. Zhang, A. Kadrolkar, and F. C. Sup, “Design and Preliminary Evaluation of a Passive Spine Exoskeleton,” Journal of Medical Devices, vol. 10, no. 1, Nov. 2015, doi: https://doi.org/10.1115/1.4031798.

[6] S. Rol, Taal, and Yoshiyuki Sankai, “Exoskeletal Spine and Shoulders for Full Body Exoskeletons in Health Care,” Advances in Applied Science Research, vol. 2, no. 6, Jan. 2011.

[7] M. B. Näf, A. S. Koopman, S. Baltrusch, C. Rodriguez-Guerrero, B. Vanderborght, and D. Lefeber, “Passive Back Support Exoskeleton Improves Range of Motion Using Flexible Beams,” Frontiers in Robotics and AI, vol. 5, p. 72, Jun. 2018, doi: https://doi.org/10.3389/frobt.2018.00072.

[8] R. Rockenfeller, “Three-dimensional spinal shape changes during daily activities,” Computers in Biology and Medicine, vol. 164, p. 107236, Jul. 2023, doi: https://doi.org/10.1016/j.compbiomed.2023.107236.

[9] The MathWorks, Inc. (2022). MATLAB version: 9.13.0 (R2022b). Accessed: January 01, 2023. Available: https://www.mathworks.com

[10] “Mokka - Motion Kinematic and Kinetic Analyzer,” biomechanical-toolkit.github.io. https://biomechanical-toolkit.github.io/mokka/

[11] X. Yong, Z. Yan, C. Wang, C. Wang, N. Li, and X. Wu, “Ergonomic Mechanical Design and Assessment of a Waist Assist Exoskeleton for Reducing Lumbar Loads During Lifting Task,” Micromachines, vol. 10, no. 7, p. 463, Jul. 2019, doi: https://doi.org/10.3390/mi10070463.

[12] Headway Batteries, "40152S LiFePO4 Cell," Headway Headquarters, 2023. [Online]. Available: https://www.headway-headquarters.com/product/40152s-3-2v-17ah-lifepo4-cell/
[13] S. Wang, Y. Zhao, and L. Chen, "A Review of Lithium-Ion Battery Safety Concerns: The Issues, Strategies, and Testing Standards," Advanced Energy Materials, vol. 10, no. 39, 2020. [Online]. Available: https://link.springer.com/article/10.1007/s42154-023-00226-3
[14] Adafruit Industries, "DC/DC Step-Down Converter - 5V @ 3A," 2023. [Online]. Available: https://www.adafruit.com/product/1385
[15] Arduino, "Arduino Uno Rev3," 2023. [Online]. Available: https://www.arduino.cc/en/Main/ArduinoBoardUno
[16] REI Co-op, "Gregory Nano 22 H2O Hydration Pack," 2023. [Online]. Available: https://www.rei.com/product/218023/gregory-nano-22-h2o-hydration-pack
[17] The Biomechanical Toolkit, "Mokka - Motion Kinematic and Kinetic Analyzer," 2023. [Online]. Available: https://biomechanical-toolkit.github.io/mokka/
[18] G. Zhu, M. Wang, and H. Liu, "Comparison of lithium iron phosphate and nickel manganese cobalt batteries for electric vehicle applications," eTransportation, vol. 15, p. 100249, Dec. 2022. [Online]. Available: https://doi.org/10.1016/j.etran.2022.100249
[19] M. F. Ashby and K. Johnson, *Materials and Design: The Art and Science of Material Selection in Product Design*, 3rd ed. Butterworth-Heinemann, 2014.
[20] A. Das and R. Alagirusamy, *Technical Textile Yarns: Industrial and Medical Applications*. Woodhead Publishing, 2010.
[21] Dassault Systèmes, "SOLIDWORKS 2023 – 3D CAD Design Software." [Online]. Available: https://www.solidworks.com/
[22] R. W. Erickson and D. Maksimović, *Fundamentals of Power Electronics*, 2nd ed. Springer, 2001.
[23] T. L. Saaty, "How to make a decision: The analytic hierarchy process," European Journal of Operational Research, vol. 48, no. 1, pp. 9–26, Sep. 1990. [Online]. Available: https://doi.org/10.1016/0377-2217(90)90057-I
[24] J. Juvinall and K. Marshek, *Fundamentals of Machine Component Design*, 6th ed., Wiley, 2016.
[25] S. Yang, B. Zhang, and H. Asada, "Design of wearable exoskeletons: A review of materials, structures, and ergonomics," IEEE Transactions on Medical Robotics and Bionics, vol. 2, no. 2, pp. 131–145, 2020.
[26] N. Bogduk, *Clinical Anatomy of the Lumbar Spine and Sacrum*, 5th ed., Churchill Livingstone, 2012.
[27] M. P. de Looze, T. Bosch, F. Krause, K. S. Stadler, and L. W. O'Sullivan, "Exoskeletons for industrial application and their potential effects on physical work load," *Ergonomics*, vol. 59, no. 5, pp. 671–681, 2016.
[28] A. J. Young and D. P. Ferris, "Ergonomics of wearable robotic exoskeletons: A review of design principles and ergonomic modeling," *Applied Ergonomics*, vol. 85, p. 103028, 2020.
[29] A. A. White and M. M. Panjabi, *Clinical Biomechanics of the Spine*, 2nd ed., Lippincott Williams and Wilkins, 1990.
[30] B. Toloyan, J. Edilson, and M. Behal, "A survey on wearable lower limb exoskeletons for gait training," *IEEE Access*, vol. 10, pp. 80235–80254, 2022.